Three-Dimensional-Printed Sensing Samples Embedding Fiber Bragg Gratings: Metrological Evaluation of Different Sample Materials and Fiber Coatings

Davide Paloschi, *Graduate Student Member, IEEE*, Andrea Polimadei, Sanzhar Korganbayev, *Graduate Student Member, IEEE*, Valerio Orsetti, Cristina Mazzotta, Alfredo Cigada, *Member, IEEE*, Michele Arturo Caponero, and Paola Saccomandi, *Senior Member, IEEE*

***Abstract*— Embedding optical fibers with fiber Bragg grating (FBG) sensors in 3-D-printed samples can effectively facilitate the systematic use of smart materials in many fields, such as civil, biomedical, and soft robotics applications. The aim of this study is to analyze different combinations of filament materials and FBG coatings and to assess their metrological characteristics. Eighteen samples are fabricated and tested under different mechanical and thermal conditions. The repeated tests allow to perform an evaluation of the measurement repeatability for each sample, along with an analysis of the sample's sensitivity. The filaments employed are acrylonitrile butadiene styrene (ABS), polylactic acid (PLA), and thermoplastic polyurethane (TPU). The fiber coatings are acrylate, Ormocer,[1] and polyimide. Results indicate that the fiber coating has no sigificative influence on the performance of the sensors. The tests for temperature sensitivity highlight a good performance of ABS (116 pm/°C) and TPU samples (32 pm/°C) up to 60 °C, whereas the fabricated PLA samples (139 pm/°C for polyimide, 55 pm/°C for acrylate, and 14 pm/°C for Ormocer[1]) cannot be used above 40 °C. The tests for strain sensitivity in axial elongation show an average sensitivity of 3.049 nm/mm for ABS, 1.991 nm/mm for PLA, and 3.726 nm/mm for TPU. The bending tests show that all specimen materials have different sensitivities to elongation (2.994 nm/mm for ABS, 0.668 nm/mm for PLA, and 0.149 nm/mm for TPU). Only for acrylate in PLA samples, an effective difference for bending sensitivity resulted (1.241 nm/mm for the acrylate coating versus 2.366 nm/mm for the other coatings).**

***Index Terms*— 3-D print, embedding, fiber Bragg grating (FBG) sensors, fiber coating, filament material, metrological characterization, sensitivity analysis, smart material.**

Manuscript received 19 December 2022; revised 1 March 2023; accepted 31 March 2023. Date of publication 20 April 2023; date of current version 5 May 2023. This work was funded by the Fondazione Cariplo under Grant No. 2017-2075. The Associate Editor coordinating the review process was Dr. Chi-Hung Hwang. *(Corresponding author: Paola Saccomandi.)*

Davide Paloschi, Sanzhar Korganbayev, Alfredo Cigada, and Paola Saccomandi are with the Department of Mechanical Engineering, Politecnico di Milano, 20156 Milan, Italy (e-mail: davide.paloschi@polimi.it; sanzhar.korganbayev@polimi.it; alfredo.cigada@polimi.it; paola.saccomandi@polimi.it).

Andrea Polimadei and Michele Arturo Caponero are with the Photonics Micro- and Nanostructures Laboratory, Research Centre of Frascati, ENEA, Frascati, 00042 Rome, Italy (e-mail: andrea.polimadei@enea.it; michele.caponero@enea.it).

Valerio Orsetti was with the FSN-TECFIS-MNF Department at ENEA Research Center of Frascati, Frascati, 00044 Rome, Italy. He is now with DTT S.c.a.r.l, 00044 Frascati, Italy (e-mail: valerio.orsetti@enea.it).

Cristina Mazzotta is with the Fusion and Technologies for Nuclear Safety and Security Department, Research Centre of Frascati, ENEA, Frascati, 00044 Rome, Italy (e-mail: cristina.mazzotta@enea.it).

Digital Object Identifier 10.1109/TIM.2023.3268466

[1]Registered trademark.

I. Introduction

MONITORING systems based on optical fiber sensors are gaining increasing attention in the fields of strain and temperature sensing due to their unique advantages that make them suitable to be used in diverse engineering applications. Some of these properties are immunity to external electromagnetic fields, small dimensions (40–250 μm diameter), low mass, ease of attachment, possibility to work in harsh environments, no voltage or current flow in the fiber, robustness, and multiplexing capabilities [1], [2], [3], [4], [5]. Sensing with optical fibers is distributed when it relies on the Brillouin or Rayleigh scatterings [6], [7], whereas it is quasi-distributed if it is based on the fiber Bragg grating (FBG) approach [8] with multipoint arrays of fiber optic sensors [9]. Both distributed and quasi-distributed systems require a single interrogation unit to be monitored, and sensors can be easily embedded in the object to be monitored. One of the main challenges with fiber optic sensors, especially for strain measurement, is the necessity to guarantee a good adhesion and mechanical match between the sensitive element and the object under test [10], [11], [12], [13]. The role of epoxy-based adhesives for structural health monitoring is analyzed in [14], [15], [16], and [17], where different adhesives are compared.

Attaching the optical sensor directly on a surface with adhesive materials leads to a contact of the sensing fiber and the monitored structure which can be affected by layer/edge effects, introducing an error in the strain transfer [17], [18]. External gluing of the fiber is also heavily dependent on the encapsulated length and on the nonuniformity of the adhesive materials (e.g., the thickness of the adhesive layer) [17].

As optical fiber sensors can be easily embedded in different structures (rigid and flexible), several recent studies investigate the possibility of embedding optical fibers

inside 3-D-printed materials. In this way, it is possible to insert the fiber in the object during the printing process and to customize the position of the sensor inside the material [19], [20], [21], [22], [23], [24], [25].

Additive manufacturing (AM) is the process of creating an object by deposition of material, layer by layer. The main techniques for AM that are commercially available are fused deposition modeling (FDM), stereolithography (SLA), and selective powder sintering (SLS). Among these processes, FDM is the most user-friendly and widely adopted technique. The filaments commonly employed by FDM printers are acrylonitrile butadiene styrene (ABS), polylactic acid (PLA), and thermoplastic polyurethane (TPU).

The available literature presents various applications for 3-D-printed sensors encapsulating optical fibers. Some notable examples are monitoring of soil deformation [23], [26], [27] and structural health [14], [16], [28], [29], [30], shape sensing [21], [31], pressure evaluation [14], [24], [26], [32], [33], [34], [35], [36], monitoring of prosthetic limbs [37], [38], and wearables for the measurement of physiological parameters, such as joint angles [39], heart rate, and respiratory rate [22]. Due to the wide spectrum of potential applications, the shape and the material of the 3-D-printed samples have usually been chosen ad hoc for the specific purpose. The shape of the sensor, the material of the filament, the infill geometry, and the infill density are parameters that heavily influence the performance of the sensor. The effect of different infills is analyzed in several studies [22], [27], [35], [36], [40], where the mechanical and thermal properties of the sensor are shown to vary according to infill density and geometry. Embedding the fiber during the 3-D printing process is preferable to gluing it in a second moment or on the external surface, since the embedding process ensures a consistent bond between the surfaces and yields a better measurement accuracy [41], [42].

Another crucial parameter that should be considered when embedding fiber optic sensors inside hosting materials is the coating of the fiber. Indeed, it has been recognized the importance of controlling the interface between the optical fiber and the material to maximize the mechanical and thermal performances of the smart material [11], [20], [43]. The optical fiber strain is generally different from the strain of the surrounding material due to the shear deformation in the coating of the fiber [10]. For this reason, the study of the behavior of different fiber coatings is necessary. In addition, the measurement sensitivity of the fiber optic sensor is also affected by the bonding length [17], [44] and adhesive thickness [45]. Fiber coatings for chemical protection are analyzed in [29], where the aim is the control of the surface properties of the fibers for the embedding in cement.

Some technical aspects should be considered in this process. For instance, when encapsulating optical fiber inside 3-D-printed materials, the embedded portion of the fiber is no longer accessible for maintenance. This problem is anyway not relevant, since the nonaccessible section near the FBG is short enough to not be able to be spliced in case of ruptures even if it was reachable. In case of failures, the patch has to be replaced with a new one, which is the same outcome as if a glued fiber were to break near the FBG location.

TABLE I
PRINTER SETTINGS AND FILAMENT SPECIFICATIONS

Parameter	ABS	PLA	TPU
Printing temperature	270 °C	200 °C	220 °C
Layer height	0.12 mm	0.12 mm	0.12 mm
Infill density	100 %	100 %	100 %
Print speed	60 mm/s	60 mm/s	30 mm/s
Wall line count	8	8	8
Vicat softening	100 °C	60 °C	113 °C
Tensile strength	38 MPa	70 MPa	45 MPa
E-Modulus	1900 MPa	3120 MPa	22 MPa

Parameters set in the slicing software of the 3D printer and main technical properties of the materials.

Different filament materials for 3-D printing possess different mechanical and thermal properties; therefore, several combinations of filaments and fiber coatings should be investigated. The main limitation of the current literature on the topic is the lack of a systematic comparison between sensors printed with different filament material hosting fibers with different coatings. For these reasons, this study presents the thermal and mechanical tests performed on eighteen 3-D-printed sensors, where all the combinations of three filament materials (ABS, PLA, and TPU) with three different fiber coatings (acrylate, Ormocer,[1] and polyimide) are considered.

II. MATERIALS AND METHODS

An FBG is the periodic modulation of the refraction index of a short segment of the optical fiber's core along its length. When broadband light is launched in the fiber, the FBG reflects a narrowband component with mean value λ_B, called the Bragg wavelength. Assuming a sine modulation, the Bragg wavelength is dependent on the effective refractive index n_{eff} (a representative value for the segment with modulated refraction index) and on the grating period λ (the distance between two consecutive regions with modified refraction index). The relationship between these parameters is reported in the following equation:

$$\lambda_B = 2 \cdot n_{\text{eff}} \cdot \lambda \tag{1}$$

The Bragg wavelength λ_B is sensitive to mechanical strain and temperature variation, as shown in the following equation:

$$\frac{\Delta\lambda_B}{\lambda_B} = P_e \cdot \varepsilon + [P_e \cdot \alpha + \xi] \cdot \Delta T \tag{2}$$

where ε is the mechanical strain, ΔT is the temperature variation, P_e is the strain-optic coefficient, α is the thermal expansion coefficient of the fiber, and ξ is the thermo-optic coefficient of the optical fiber.

Eighteen samples of optical fibers embedded in 3-D-printed material were produced and tested. The 3-D-printed materials that were used are ABS, PLA, and TPU. The samples were created with the X-Max 3-D printer (QIDI tech). The relevant printing parameters are reported in Table I.

The coatings of the optical fibers that were selected are acrylate, Ormocer,[1] and polyimide, which are characterized by an E-modulus of 7, 1500, and 4900 MPa, respectively. Each fiber housed one FBG, characterized by 10, 8, and 5 mm

TABLE II
LIST OF SAMPLES

Patch number	Identifier	Filament material	Fiber coating
1	ABS_A_1	ABS	Acrylate
2	ABS_A_2	ABS	Acrylate
3	ABS_O_1	ABS	Ormocer®
4	ABS_O_2	ABS	Ormocer®
5	ABS_P_1	ABS	Polyimide
6	ABS_P_2	ABS	Polyimide
7	PLA_A_1	PLA	Acrylate
8	PLA_A_2	PLA	Acrylate
9	PLA_O_1	PLA	Ormocer®
10	PLA_O_2	PLA	Ormocer®
11	PLA_P_1	PLA	Polyimide
12	PLA_P_2	PLA	Polyimide
13	TPU_A_1	TPU	Acrylate
14	TPU_A_2	TPU	Acrylate
15	TPU_O_1	TPU	Ormocer®
16	TPU_O_2	TPU	Ormocer®
17	TPU_P_1	TPU	Polyimide
18	TPU_P_2	TPU	Polyimide

Complete list of the combinations of coatings of the fibers and filaments of the samples.

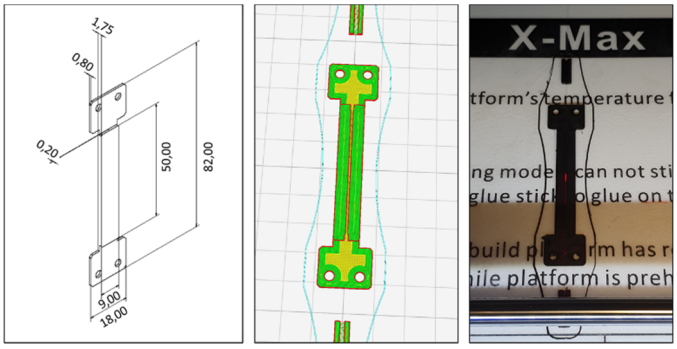

(a) (b) (c)

Fig. 1. Design and fabrication. (a) Three-dimensional model of the patch designed in Autodesk Inventor. (b) View of the slicing software (QIDI Print) of the layer where the printing process has to be paused and the fiber has to be placed. (c) Location of the FBG in the fiber is identified with a pilot laser. The exemplifying picture shows a PLA-based 3-D-printed sensor.

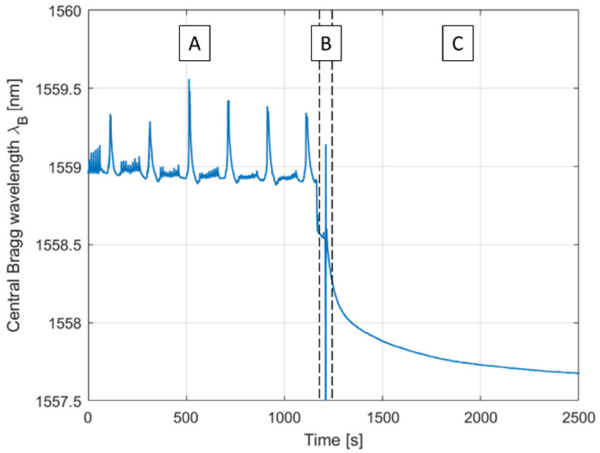

Fig. 2. Value of λ_B monitored during the embedding of the fiber in the 3-D-printed patch. Zone A of the graph shows the response of the fiber to the extruder of the printer creating the top layers. Zone B is the removal of the tensioning weights and the detachment of the printing plate from the base of the printer when the process is complete. Zone C is the cooling phase of the sample.

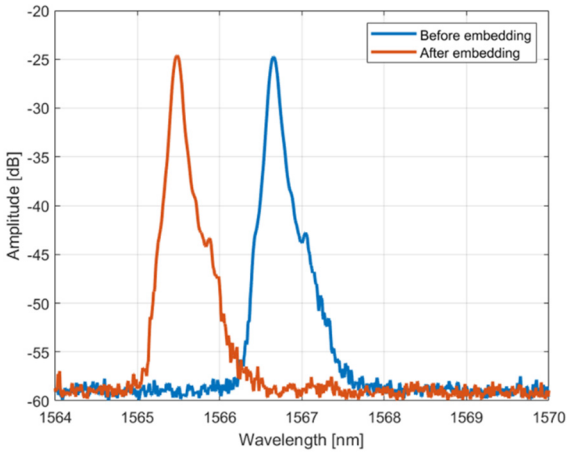

Fig. 3. Central Bragg wavelength (λ_B). The spectrum shifts to the left after the fiber is embedded and the patch cools down.

sensitive length, respectively. The different sensing length is related to different producers of the fibers and does not have any influence on the results of the tests, as long as the sensing part is completely encapsulated in the material. Moreover, the four-point bending test ensures a constant strain profile in the sensing area of the sample. Two samples per each combination were produced, as reported in Table II. The 3-D model of the sample is shown in Fig. 1.

The 3-D-printed samples have been designed with a central groove for the fiber positioning. The samples have an overall length of 82 mm and maximum width of 18 mm in correspondence of the extremities, where four holes were designed for the screwing of the sample for future applications. The body of the sensor is 9 mm in width, and the size of the groove for the optical fiber is 0.3 mm in width and 0.2 mm in height. Details are reported in Fig. 1(a).

The following fabrication procedure has been implemented: 1) the printing process was halted at the end of the last layer containing the channel for the fiber and 2) the optical fiber was then placed on the semi-finished print with the help of a pilot laser (low power laser in the visible range) to ensure a correct positioning of the FBG with respect to the patch (i.e., FBG region at the center of the 3-D-printed structure), as shown in Fig. 1(c). Finally, the printing process was resumed, and the FBG-embedded 3-D-printed patches were fabricated.

A magnetic weight of 45 g was clamped on the fiber on both sides of the plate of the printer, in order to pretension the fiber before the embedding process. The fiber was then connected to the optical interrogator (HYPERION si255, Atlanta, USA) to monitor the shift of Bragg wavelength during the embedding phase, as shown in Figs. 2 and 3. The complete sensor is now sensitive as a unique item (tensioned fiber embedded in the filament material) to the magnetic weights.

The removal of the magnetic weights caused a partial decrease in λ_B, since the sample was not under traction anymore, but the main cause for loss in λ_B was related to the cooling of the sample.

The final sensor is characterized by a lower value of λ_B in comparison with the bare fiber. This result agrees with the other works found in [20], [24], [26], [27], [30], [35], and [39] and is related to the shrinkage of the material during cooling that applies a compressive force to the fiber. The described

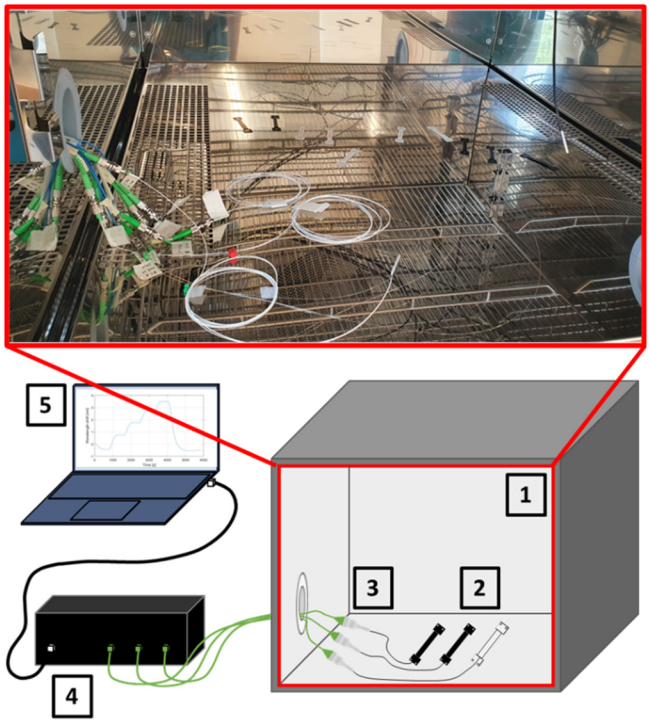

Fig. 4. Schematics of the experimental setup and picture of the thermal chamber. The samples are placed inside the chamber and connected to patch cords to reach the optical interrogator outside. 1) Thermal chamber. 2) Three-dimensional-printed samples. 3) Patch cords connecting the samples under test to the interrogator. 4) Interrogator (HYPERION si255). 5) Laptop connected to the interrogator for data acquisition.

fabrication process has been repeated for all the combinations listed in Table II. For all the samples, the Central Bragg wavelength has been monitored during the embedding process. Figs. 2 and 3 show the exemplifying behavior of a single patch for the sake of conciseness. The 3-D-printed sensors have been tested for both thermal and mechanical properties.

A. Thermal Tests

The samples were placed in a thermal chamber. The experiment was carried out with a stepwise temperature increase and a continuous temperature decrease. The temperature setpoints selected for the test were 20 °C, 30 °C, 40 °C, 50 °C, and 60 °C. The time delay between each setpoint was set to 10 min. Then, the set temperature was decreased from 60 °C to 20 °C.

Three not-embedded FBGs, one per type of coating (acrylate, Ormocer,[1] and polyimide), were also placed in the chamber for reference, to measure the different sensitivities with respect to the embedded sensors. FBGs were interrogated by the HYPERION si255 optical interrogator and sampled at a frequency of 1 Hz. The experimental setup is shown in Fig. 4.

B. Mechanical Tests

The sensorized patches have been tested for mechanical strain using the Z5 traction machine (Thümler GmbH), with a load cell having a full scale of 50 N and a sampling rate of 50 Hz. The optical interrogation unit used to sample the response of the sensors is the Hottinger Baldwin Messtechnik (HBM) Braggmeter FS2200, which saves data at a frequency of 1 Hz. The experimental setup is shown in Fig. 5.

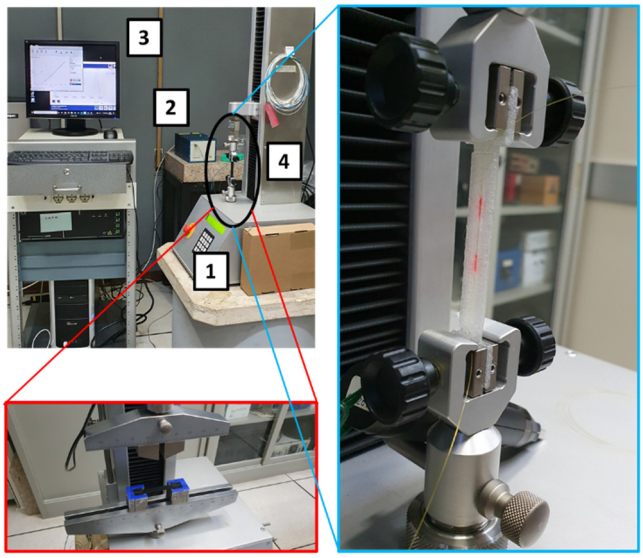

(a) (b)

Fig. 5. Experimental setup. 1) Machine used for the mechanical tests (Z5, Thümler GmbH). 2) Interrogator used during the tests (HBM Braggmeter FS2200). 3) Computer connected to the interrogator and the machine for data acquisition. 4) Load cell and sample under test. The different configurations are shown for (a) bending test and (b) tensile test.

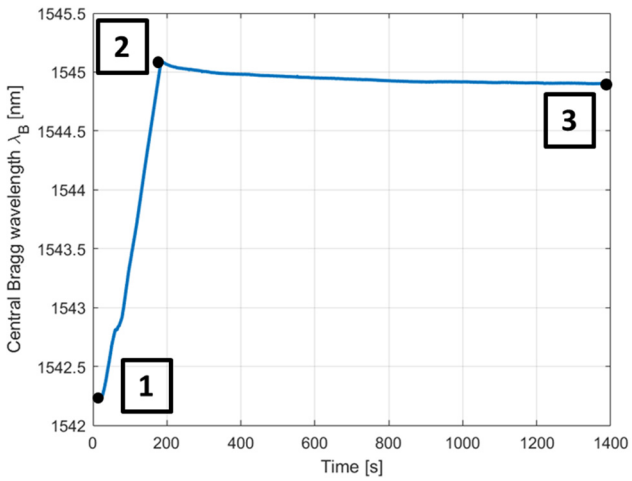

Fig. 6. Example of stability test. 1) Wavelength at the starting condition $\lambda_B(1)$. 2) Wavelength at the maximum displacement $\lambda_B(2)$. 3) Wavelength after 20 min $\lambda_B(3)$.

One sample per type was tested for long-term performance in the tensile test, as shown in Fig. 6. A displacement of 1.5 mm was applied, and the sample was held in the same position for 20 min, after which the readings were evaluated using the percentual variation reported in the following equation:

$$\text{Loss} = \frac{\lambda_B(2) - \lambda_B(3)}{\lambda_B(2) - \lambda_B(1)} \tag{3}$$

where $\lambda_B(1)$ is the central Bragg wavelength at the beginning of the test, $\lambda_B(2)$ is when first reaching the maximum displacement imposed by the tensile machine, and $\lambda_B(3)$ is after 20 min in stationary conditions, as shown in Fig. 6.

Also, the samples underwent periodic tensile and bending tests.

The four-point bending test guarantees the strain to be uniform between the application points of the load. For this reason, the uncertainty in the exact location of the FBG is

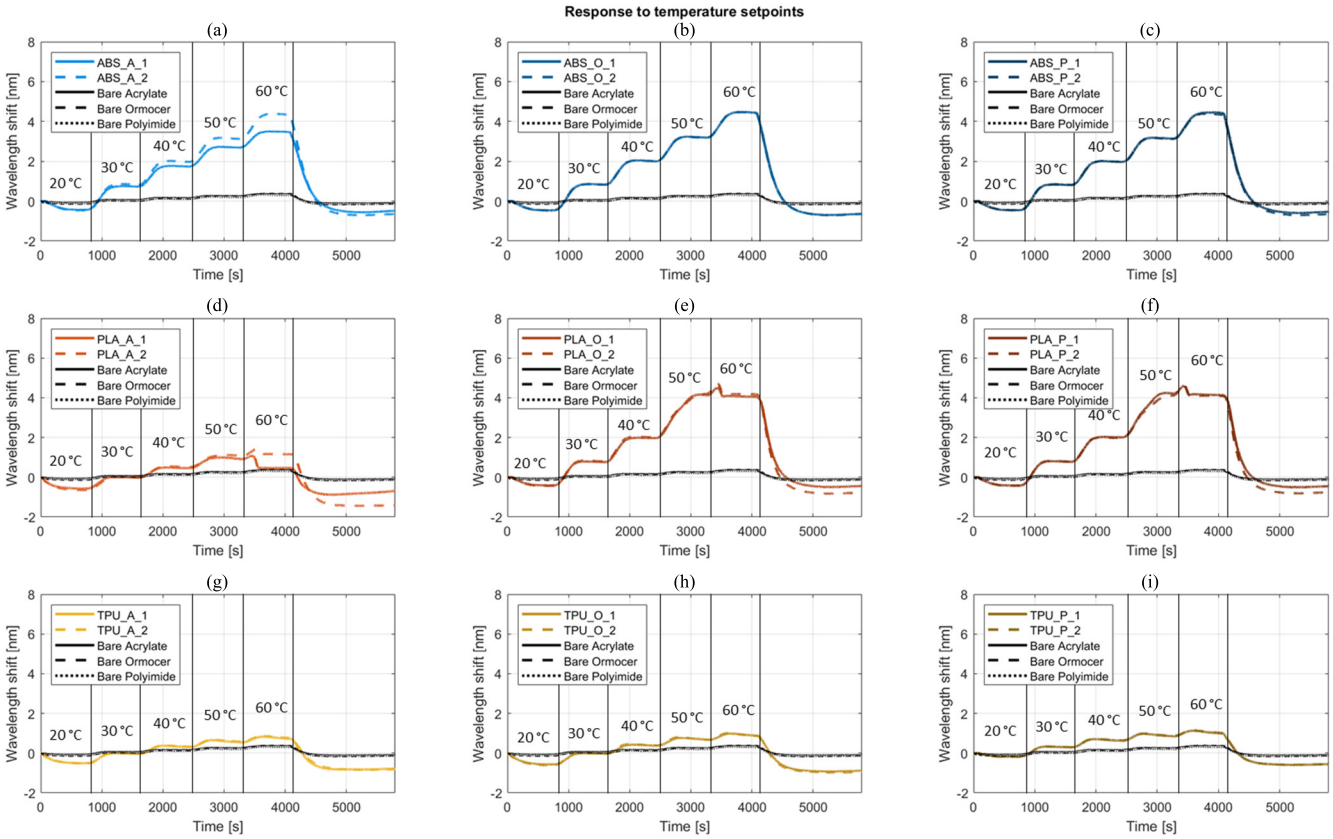

Fig. 7. Thermal test. (a) Response of the ABS samples with acrylate coating. (b) Response of the ABS samples with Ormocer[1] coating. (c) Response of the ABS samples with polyimide coating. (d) Response of the PLA samples with acrylate coating. (e) Response of the PLA samples with Ormocer[1] coating. (f) Response of the PLA samples with polyimide coating. (g) Response of the TPU samples with acrylate coating. (h) Response of the TPU samples with Ormocer[1] coating. (i) Response of the TPU samples with polyimide coating. The measurements with the bare fibers are reported in black solid line (acrylate), black dashed line (Ormocer[1]), and black dotted line (polyimide). The temperature setpoint of the thermal chamber is numerically reported in each zone.

TABLE III
TENSILE TEST

Symbol	ABS and PLA	TPU
Starting condition	30 N	1.5 mm
Machine speed	0.1 mm/min	0.1 mm/min
Imposed extension	0.1 mm	0.1 mm
Repetitions	11	11

Parameters set in the software of the machine for the tensile test.

TABLE IV
BENDING TEST

Symbol	ABS and PLA	TPU
Starting condition	0.1 mm	0.5 mm
Machine speed	0.1 mm/min	0.1 mm/min
Imposed deformation	1 mm	3 mm
Repetitions	11	11

Parameters set in the software of the machine for the bending test.

not relevant as long as it remains in the region between the application points. The parameters of the tests are listed in Tables III and IV.

The starting condition refers to the load or displacement that is applied to the sample by the tensile machine in order to tension it before starting the periodic test.

The values of Bragg wavelength, applied load, and displacement are analyzed at the starting of each repetition and at the maximum imposed deformation of each cycle. The sensitivity over load (shift/load) is defined as the ratio, for each cycle, of the peak-to-peak load. Mean and standard deviation are calculated on these values for a general description of the sample. The sensitivity over stroke (shift/stroke) is defined as the ratio, for each cycle, of the peak-to-peak wavelength over the peak-to-peak way.

III. RESULTS AND DISCUSSION

A. Thermal Tests

The results of the thermal tests are reported in Fig. 7 for all the samples. The initial reduction in λ_B is due to the cooling of the chamber, as the first temperature setpoint (20 °C) was lower than the ambient temperature. The final value of λ_B, which is supposed to be measured at 20 °C, is lower than the value measured in the beginning of the test with the same setpoint. This effect is related to the temperature control of the machine, which overshoots in order to react in a faster way to large setpoint changes.

The ABS samples show a good response to temperature variations within the selected measurement range, i.e., 20 °C–60 °C [Fig. 7(a)–(c)]. The sensitivity to temperature is enhanced by an order of magnitude with respect to a

TABLE V
PERCENTUAL LOSS OVER TIME

Identifier of the patch	Loss [%]
ABS_A_1	21.8
ABS_O_1	11.3
ABS_P_1	16.7
PLA_A_1	11.3
PLA_O_1	17.9
PLA_P_1	14.3
TPU_A_1	13.3
TPU_O_1	6.8
TPU_P_1	6.1

Percentual difference of reading after holding the same displacement for twenty minutes during a tensile test.

bare fiber (in the range 20 °C–60 °C, the mean temperature sensitivity is 116 pm/°C, whereas the mean sensitivity of the bare fibers is 11 pm/°C). The PLA samples with polyimide coating present the highest sensitivity to temperature (in the range 20 °C–40 °C, the mean temperature sensitivity is 120 pm/°C). These results are comparable with the outcome of previous studies, which reported a temperature sensitivity of 139 pm/°C for PLA structures embedding FBGs [19]. The mean temperature sensitivity of the PLA samples with acrylate coating is 55 pm/°C, whereas the mean temperature sensitivity of the PLA samples with Ormocer[1] coating is 14 pm/°C. In the configuration tested in our work, our PLA samples result to be not suitable for temperatures above 40 °C. In fact, as it is visible in the graph [Fig. 7(d)–(f)], the wavelength shift measured by the samples becomes unreliable above that value. Most likely, the material becomes too much malleable and the adherence with the embedded fiber decreases, changing the properties of the sensor. This result is coherent with the proximity to Vicat softening of PLA (60 °C).

The TPU samples shown the lowest temperature sensitivity, regardless of the FBG coating (in the range 20 °C–60 °C, the mean temperature sensitivity is 31 pm/°C for the acrylate coating, 36 pm/°C for the Ormocer[1] coating, and 29 pm/°C for the polyimide coating). This response may be explained by the low-temperature expansion coefficient, and by the material anisotropy, which might induce a nonuniform strain field on the grating when the temperature increases [19]. Moreover, the setpoint tracking has a longer setting time and a more visible initial overshoot with the increase of temperature [Fig. 7(g)–(i)].

B. Mechanical Tests

The results for the long-term stability tests are reported in Table V.

Overall, ABS samples exhibit the largest loss over time, whereas TPU samples are characterized by a small percentual loss. The decreasing trend in the measurement is related to the relaxation of the material over time.

The measurements of a subset of 3-D-printed samples (i.e., a single patch with polyimide coating per type of filament material) are reported in Fig. 8. The measurements belong to

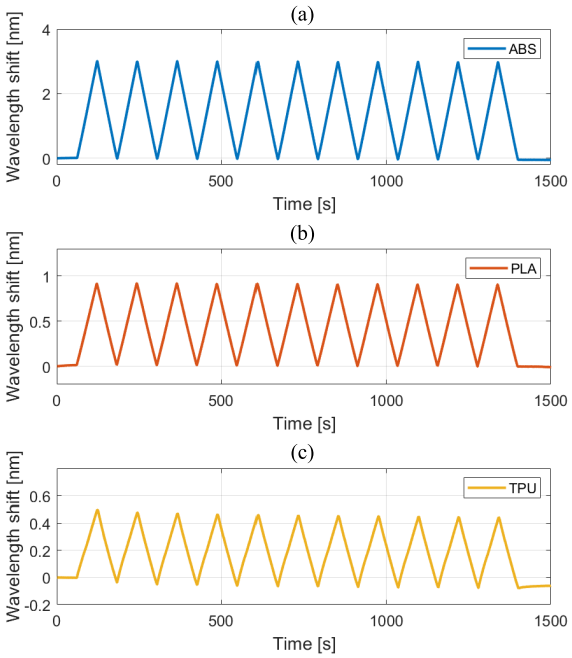

Fig. 8. Mechanical tests (bending). (a) Response of an ABS patch. (b) Response of a PLA patch. (c) Response of a TPU patch. The coating of the fiber is polyimide for all of the presented results.

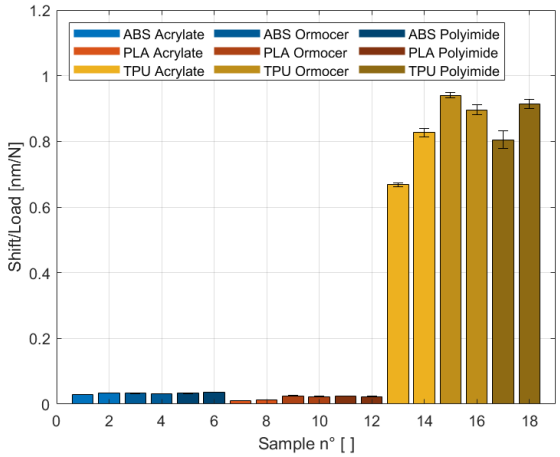

Fig. 9. Average shift/load sensitivity of each patch during tensile test. The wavelength shift measured by the FBG is divided by the maximum load applied to the patch at each repetition. Each bar of the graph is the averaged value of a single patch.

the bending test, whereas the tensile test is not reported for the sake of conciseness, as it has analogous readings.

As clearly visible in Fig. 8(c), the ending point does not coincide exactly with the starting one. This phenomenon is caused by material relaxation, as already reported in Table V for the long-term testing. For this reason, the performance of the samples will now be evaluated by considering the starting and ending point of each cycle of the periodic test. This method analyzes the repeatability of the measurement.

The results of the sensitivity analysis for the tensile tests are reported in Figs. 9 and 10. The maximum displacement in both the tensile and bending tests indicates the deformation that the machine imposes to the sample during the periodic tests. The

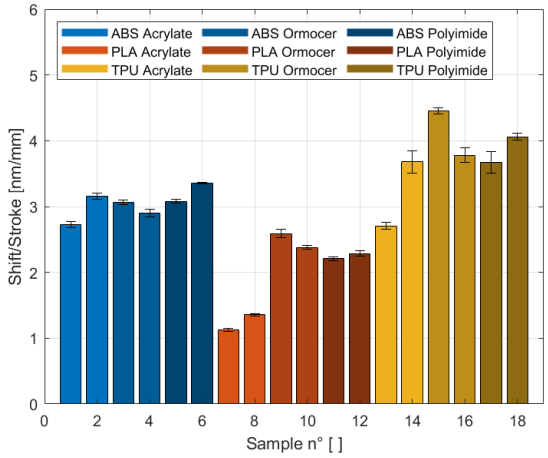

Fig. 10. Average shift/stroke sensitivity of each patch during tensile test. The wavelength shift measured by the FBG is divided by the maximum displacement enforced by the machine at each repetition. Each bar of the graph is the averaged value of a single patch.

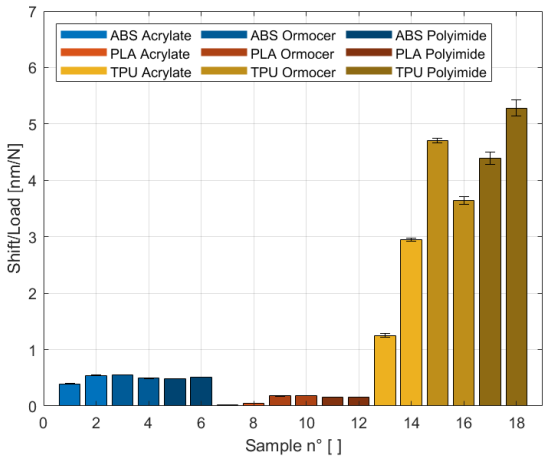

Fig. 11. Average shift/load of each patch during bending test. The wavelength shift measured by the FBG is divided by the maximum load applied to the patch at each repetition. Each bar of the graph is the averaged value of a single patch.

maximum load is the force that the load cell of the machine measures when the maximum displacement is reached.

The ABS samples present a coherent mean sensitivity value across all the different fiber coatings (i.e., from 0.029 to 0.037 nm/N). The PLA samples have a similar behavior, with only the acrylate-coated fibers (Sample 7 PLA_A_1 and Sample 8 PLA_A_2) presenting a lower mean sensitivity value (i.e., 0.011 and 0.013 nm/N). The TPU material is for sure more elastic than ABS and TPU. Indeed, the mean sensitivity of the TPU samples over the load of the machine is greater than the ABS and PLA counterparts, because the material easily elongates even at low forces (i.e., an average of 0.842 nm/N for the TPU versus 0.033 nm/N for the ABS and 0.020 nm/N for the PLA).

The sensitivity of the samples over the sample elongation is more coherent across the different filament materials than the one over load. The PLA samples with acrylate coating (Sample 7 PLA_A_1 and Sample 8 PLA_A_2) have a lower sensitivity than the PLA samples with Ormocer[1] and polyimide coatings (Sample 9 PLA_O_1, Sample 10 PLA_O_2, Sample 11 PLA_P_1, and Sample 12 PLA_P_2), as already seen in the sensitivity over load in Fig. 9 (i.e., an average of 1.241 nm/mm for the acrylate coating versus 2.366 nm/mm for the other coatings). The TPU samples have different mean sensitivities from sample to sample, with an average value compatible with the ABS samples (i.e., 3.726 versus 3.049 nm/mm).

The results of the bending tests are reported in Figs. 11 and 12. The shift/load values measured in the bending tests show a behavior similar to the tensile tests. The ABS samples have similar sensitivity values among samples (i.e., 0.496 $\pm$ 0.002 nm/N). The PLA samples with acrylate coating (Sample 7 PLA_A_1 and Sample 8 PLA_A_2) have a lower average sensitivity than the samples with different coatings (i.e., 0.037 versus 0.168 nm/N). The higher sensitivity of ABS patches with respect to PLA patches during four-point bending test was also reported in [20]. The TPU samples show a behavior which greatly differs from sample to sample. The sensitivity of the TPU samples is again larger than the one

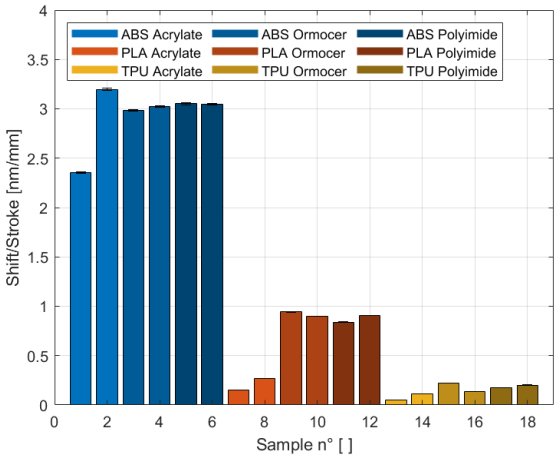

Fig. 12. Average shift/stroke of each sample during bending test. The wavelength shift measured by the FBG is divided by the maximum displacement enforced by the machine at each repetition. Each bar of the graph is the averaged value of a single sample.

of the other materials, because it can be easily deformed with small loads (i.e., an average of 3.702 nm/N for the TPU versus 0.496 nm/N for the ABS and 0.124 nm/N for the PLA).

The average sensitivity over displacement of the ABS samples is greater than the sensitivity of the other samples due to the stiffness of the material and the bond between fiber and sample (i.e., an average of 2.944 nm/mm for the ABS versus 0.668 nm/N for the PLA and 0.149 nm/N for the TPU).

The difference in λ_B of each sensor after usage is reported in Table VI.

The majority of the samples experience a negative shift of Bragg wavelength after usage. A negative shift of the Bragg wavelength is related to the compression of the fiber inside the patch, whereas a positive shift of the Bragg wavelength is related to the tension of the fiber. This effect is due to the plasticity of the materials and to the setting of the fiber inside the patch. The TPU samples exhibit low variations after being tested thanks to their higher elasticity. The only exception is the tensile test of Sample 16 TPU_O_2, where the shift is very

TABLE VI
WAVELENGTH SHIFT AFTER TESTS

Identifier of the patch	Tensile [pm]	Bending [pm]
ABS_A_1	-20	-115
ABS_A_2	-320	-575
ABS_O_1	-150	-330
ABS_O_2	-165	-190
ABS_P_1	35	85
ABS_P_2	-40	-65
PLA_A_1	-35	105
PLA_A_2	-10	-40
PLA_O_1	160	-220
PLA_O_2	45	-240
PLA_P_1	-130	-100
PLA_P_2	-105	-185
TPU_A_1	-35	10
TPU_A_2	20	-60
TPU_O_1	-105	-40
TPU_O_2	-1000	10
TPU_P_1	225	-70
TPU_P_2	15	-30

Difference in λ_B before and after the testing of the sample. Negative values represent a left shift of λ_B.

large. This could be due to an adjustment of the fiber inside the encapsulation, forced by the tensile test.

ABS samples have high sensitivity over imposed deformations and behave consistently in the thermal tests. The large sensitivity over temperature makes them very interesting for thermal applications or for health monitoring applications. PLA samples behave like ABS samples in the tensile test, whereas they exhibit a lower sensitivity during bending tests. The thermal tests show the impossibility to use our PLA sensors in environments with more than 40 °C, limiting their application for external use. To improve the measurement range suitable for PLA samples, a possible future solution might be to adopt a different shape of the groove for the positioning of the fiber (e.g., V-groove, as performed in [19] rather than a rectangular groove as was done in our experiments).

TPU samples have high sensitivity over load in both tensile and bending tests. Their more elastic nature makes them suitable for wearable applications in the biomedical fields.

Overall, the only coating that has an effect on the performance of the sensor is acrylate. This effect is mostly visible with PLA samples, with a less important influence also on TPU samples. Similar results with acrylate coating were already observed in the literature when the fiber is glued to the surface, as it is related to slippage between coating and cladding [46]. The repeatability of the process is heavily dependent on the 3-D printer and on its maintenance status, as a minor difference during the process results in a completely different output. Furthermore, each sensor should be calibrated before being employed, since the sensitivity can vary even between samples of the same type.

C. Metrological Evaluation

The repeated mechanical tests allow to perform an evaluation of the measurement repeatability for each sample, based upon the calculated standard deviation.

The results of the tensile tests in terms of shift/load (Fig. 9) show that, for ABS, there is no relevant difference among samples embedding FBGs with different coatings. In particular, the overall ABS shift/load tensile sensitivity is 0.033 ± 0.002 nm/N. The PLA shift/load tensile sensitivity is 0.012 ± 0.002 nm/N for acrylate coating (Sample 7 PLA_A_1 and Sample 8 PLA_A_2) versus 0.024 ± 0.001 nm/N for the other PLA samples. For the TPU, a largest difference among different samples is observed. Indeed, the overall TPU shift/load tensile sensitivity is 0.842 ± 0.100 nm/N, with a minimum of 0.668 ± 0.005 nm/N (Sample 13 TPU_A_1) and a maximum of 0.941 ± 0.008 nm/N (Sample 15 TPU_O_1).

Similar conclusions can be drawn for the shift/stroke results of the tensile tests (Fig. 10). The overall ABS shift/stroke tensile sensitivity is 3.049 ± 0.215 nm/mm. Regarding the PLA samples, Sample 7 PLA_A_1 and Sample 8 PLA_A_2 are characterized by an average shift/stroke tensile sensitivity of 1.240 ± 0.166 nm/mm which is not compatible with the other PLA samples (2.366 ± 0.166 nm/mm). The TPU overall shift/stroke tensile sensitivity is 3.726 ± 0.582 nm/mm, thus showing an evident nonuniformity among different samples, i.e., a minimum of 2.71 ± 0.056 nm/mm (Sample 13 TPU_A_1) and a maximum of 4.456 ± 0.050 nm/mm (Sample 15 TPU_O_1).

Regarding the shift/load bending sensitivity (Fig. 11), the ABS overall value is 0.496 ± 0.058 nm/N, but Sample 1 ABS_A_1 is characterized by a shift/load bending sensitivity that is not compatible with the other ABS samples (0.394 ± 0.002 versus 0.516 ± 0.032 nm/N). The PLA shift/load bending sensitivity is 0.124 ± 0.069 nm/N, but Sample 7 PLA_A_1 and Sample 8 PLA_A_2 are characterized by an average shift/load bending sensitivity of 0.037 ± 0.015 nm/N which is not compatible with the other PLA samples (0.168 ± 0.015 nm/N). The TPU shift/load bending sensitivity is 3.703 ± 1.452 nm/N, also in this case showing a large nonuniformity among the samples.

The shift/stroke results of the bending tests (Fig. 12) are discussed as follows. The ABS has an overall shift/stroke sensitivity of 2.944 ± 0.296 nm/mm, but Sample 1 ABS_A_1 is characterized by a shift/stroke bending sensitivity that is not compatible with the other ABS samples (2.357 ± 0.008 versus 3.061 ± 0.080 nm/mm). The PLA overall shift/stroke bending sensitivity is 0.669 ± 0.358 nm/mm, but Sample 7 PLA_A_1 and Sample 8 PLA_A_2 are characterized by an average sensitivity of 0.211 ± 0.084 nm/mm which is not compatible with the other PLA samples (0.897 ± 0.043 nm/mm). The TPU overall shift/stroke bending sensitivity is 0.149 ± 0.063 nm/mm, still exhibiting a slight nonuniformity among the samples.

From these results, we can conclude that the repeatability of the measurement for the single sample is always high, regardless of the material filament and the fiber coating. However, the slight differences observed for some samples (e.g., ABS and PLA with acrylate-coated FBG, and most of the TPU samples) suggest that future efforts should go toward increasing the fabrication process reproducibility.

IV. Conclusion

This work presents the fabrication and testing of eighteen 3-D-printed samples with a single embedded FBG. The samples obtained by all the combinations of three filaments (ABS, PLA, and TPU) with three fiber coatings (acrylate, Ormocer,[1] and polyimide) were tested in a thermal chamber, in a tensile test, and in a bending test. The thermal tests highlight the impossibility to use the fabricated PLA samples at temperatures above 40 °C, due to the large deformation of the material. On the other hand, both ABS and TPU samples are reliable in the range 20–60 °C.

Regarding the mechanical tests, the repeatability of the measurement for the single sample is always high, regardless of the material filament and the fiber coating. The ABS samples present a coherent behavior across all the different fiber coatings. The PLA samples with acrylate fiber coating are characterized by a lower sensitivity with respect to the ones with Ormocer[1] and polyimide fiber coatings, which are comparable. The TPU samples exhibit a variable sensitivity from sample to sample, denoting a poor reproducibility of the output of the printing process.

Future works will focus on the optimization of the production process and on the testing of these sensors in civil and biomedical applications.

Acknowledgment

The authors are thankful to Prof. Marcello Colledani and Dr. Luca Gentilini of the Department of Mechanical Engineering of Politecnico di Milano, Milan, Italy, for the use of the thermal chamber.

References

[1] A. D. Kersey et al., "Fiber grating sensors," *J. Lightw. Technol.*, vol. 15, no. 5, pp. 1442–1463, 1997.

[2] E. Udd and W. B. Spillman Jr., *Fiber Optic Sensors: An Introduction for Engineers and Scientists*. Hoboken, NJ, USA: Wiley, 2011.

[3] A. Othonos, K. Kalli, and G. E. Kohnke, "Fiber Bragg gratings: Fundamentals and applications in telecommunications and sensing," *Phys. Today*, vol. 53, no. 5, pp. 61–62, May 2000, doi: 10.1063/1.883086.

[4] D. H. Waters, J. Hoffman, and M. Kumosa, "Monitoring of overhead transmission conductors subjected to static and impact loads using fiber Bragg grating sensors," *IEEE Trans. Instrum. Meas.*, vol. 68, no. 2, pp. 595–605, Feb. 2019, doi: 10.1109/TIM.2018.2851698.

[5] J. Chen, Y. Song, F. Xiong, and T. Ai, "A thermal effects-based method for void detection in concrete face rockfill dams," *IEEE Trans. Instrum. Meas.*, vol. 71, pp. 1–7, 2022, doi: 10.1109/TIM.2021.3127638.

[6] M. E. Froggatt and R. G. Duncan, "Fiber optic position and/or shape sensing based on Rayleigh scatter," Google Patents 7 772 541, Aug. 10, 2010.

[7] M. E. Froggatt, J. W. Klein, D. K. Gifford, and S. T. Kreger, "Optical position and/or shape sensing," U.S. Patent 8 773 650 B2, Jul. 8, 2014.

[8] K. Bronnikov et al., "Durable shape sensor based on FBG array inscribed in polyimide-coated multicore optical fiber," *Opt. Exp.*, vol. 27, no. 26, p. 38421, Dec. 2019, doi: 10.1364/oe.380816.

[9] D. Paloschi, K. A. Bronnikov, S. Korganbayev, A. A. Wolf, A. Dostovalov, and P. Saccomandi, "3D shape sensing with multicore optical fibers: Transformation matrices versus Frenet–Serret equations for real-time application," *IEEE Sensors J.*, vol. 21, no. 4, pp. 4599–4609, Feb. 2021.

[10] S.-C. Her and C.-Y. Huang, "Effect of coating on the strain transfer of optical fiber sensors," *Sensors*, vol. 11, no. 7, pp. 6926–6941, Jul. 2011, doi: 10.3390/s110706926.

[11] Q. Li, G. Li, and G. Wang, "Effect of the plastic coating on strain measurement of concrete by fiber optic sensor," *Measurement*, vol. 34, no. 3, pp. 215–227, Oct. 2003, doi: 10.1016/S0263-2241(03)00052-6.

[12] F. Yu, O. Saito, and Y. Okabe, "Laser ultrasonic visualization technique using a fiber-optic Bragg grating ultrasonic sensor with an improved adhesion configuration," *Struct. Health Monitor.*, vol. 20, no. 1, pp. 303–320, Jan. 2021, doi: 10.1177/1475921720932233.

[13] O. Almubaied, H. K. Chai, M. R. Islam, K.-S. Lim, and C. G. Tan, "Monitoring corrosion process of reinforced concrete structure using FBG strain sensor," *IEEE Trans. Instrum. Meas.*, vol. 66, no. 8, pp. 2148–2155, Aug. 2017, doi: 10.1109/TIM.2017.2676218.

[14] Y. Zhang et al., "A high precision fiber optic Fabry–Perot pressure sensor based on AB epoxy adhesive film," *Photonics*, vol. 8, no. 12, p. 581, Dec. 2021, doi: 10.3390/photonics8120581.

[15] H. Tian, D.-G. Liu, Y.-P. Wang, and Q.-L. Wang, "Effect of adhesive type on the sensitivity coefficient of FBG sensor bonded on the surface of CFRP," *Optoelectron. Lett.*, vol. 15, no. 4, pp. 264–268, Jul. 2019, doi: 10.1007/s11801-019-8183-5.

[16] S. Young et al., "Smart adhesive joint with high-definition fiber-optic sensing for automotive applications," *Sensors*, vol. 20, no. 3, p. 614, Jan. 2020, doi: 10.3390/s20030614.

[17] S.-Y. Seo, J.-H. Park, H.-D. Yun, K.-S. Kim, G.-C. Lee, and S. Hong, "Strain transfer of fiber Bragg grating sensor externally bonded to FRP strip for structural monitoring after reinforcement," *Materials*, vol. 14, no. 16, p. 4382, Aug. 2021, doi: 10.3390/ma14164382.

[18] H. P. Wang, P. Xiang, and X. Li, "Theoretical analysis on strain transfer error of FBG sensors attached on steel structures subjected to fatigue load," *Strain*, vol. 52, no. 6, pp. 522–530, 2016, doi: 10.1111/str.12195.

[19] A. Leal-Junior, J. Casas, C. Marques, M. Pontes, and A. Frizera, "Application of additive layer manufacturing technique on the development of high sensitive fiber Bragg grating temperature sensors," *Sensors*, vol. 18, no. 12, p. 4120, Nov. 2018, doi: 10.3390/S18124120.

[20] P. D. Palma, A. Iadicicco, and S. Campopiano, "Study of fiber Bragg gratings embedded in 3D-printed patches for deformation monitoring," *IEEE Sensors J.*, vol. 20, no. 22, pp. 13379–13386, Nov. 2020, doi: 10.1109/JSEN.2020.3004280.

[21] P. Di Palma, E. De Vita, A. Iadicicco, and S. Campopiano, "3D shape sensing with FBG-based patch: From the idea to the device," *IEEE Sensors J.*, vol. 22, no. 2, pp. 1338–1345, Jan. 2022, doi: 10.1109/JSEN.2021.3133704.

[22] D. L. Presti et al., "The effect of infill pattern and density on the response of 3-D-printed sensors based on FBG technology," *IEEE Sensors J.*, vol. 22, no. 20, pp. 19357–19365, Oct. 2022, doi: 10.1109/JSEN.2022.3202101.

[23] M. A. Alias et al., "Highly sensitive temperature-independent FBG-based sensor embedded in thermoplastic polyurethane using 3D printing technology for the measurements of torsion," *Sens. Actuators A, Phys.*, vol. 346, Oct. 2022, Art. no. 113889, doi: 10.1016/j.sna.2022.113889.

[24] C. Hong, Y. Zhang, D. Su, and Z. Yin, "Development of a FBG based hoop-strain sensor using 3D printing method," *IEEE Access*, vol. 7, pp. 107154–107160, 2019, doi: 10.1109/ACCESS.2019.2933568.

[25] N. R. Manzo, G. T. Callado, C. M. B. Cordeiro, and L. C. M. Vieira Jr., "Embedding optical fiber Bragg grating (FBG) sensors in 3D printed casings," *Opt. Fiber Technol.*, vol. 53, Dec. 2019, Art. no. 102015, doi: 10.1016/j.yofte.2019.102015.

[26] C. Hong, Y. Zhang, Y. Yang, and Y. Yuan, "A FBG based displacement transducer for small soil deformation measurement," *Sens. Actuators A, Phys.*, vol. 286, pp. 35–42, Feb. 2019, doi: 10.1016/j.sna.2018.12.022.

[27] C. Hong, X. Wang, K. Han, D. Su, and Z. Chen, "Performance investigation of 3D printed clay soil using fiber Bragg grating technology," *Acta Geotechnica*, vol. 17, no. 2, pp. 453–462, Feb. 2022, doi: 10.1007/s11440-021-01250-5.

[28] Y. Zhao, N. Zhang, G. Si, and X. Li, "Study on the optimal groove shape and glue material for fiber Bragg grating measuring bolts," *Sensors*, vol. 18, no. 6, p. 1799, Jun. 2018, doi: 10.3390/s18061799.

[29] W. R. Habel and A. Bismarck, "Optimization of the adhesion of fiber-optic strain sensors embedded in cement matrices; A study into long-term fiber strength," *J. Struct. Control*, vol. 7, no. 1, pp. 51–76, Jun. 2000, doi: 10.1002/stc.4300070105.

[30] L. Fang, T. Chen, R. Li, and S. Liu, "Application of embedded fiber Bragg grating (FBG) sensors in monitoring health to 3D printing structures," *IEEE Sensors J.*, vol. 16, no. 17, pp. 6604–6610, Sep. 2016, doi: 10.1109/JSEN.2016.2584141.

[31] P. D. Palma, A. Iadicicco, and S. Campopiano, "Curvature sensor based on FBGs embedded in 3D printed patches," *IEEE Sensors J.*, vol. 21, no. 16, pp. 17868–17874, Aug. 2021, doi: 10.1109/JSEN.2021.3083961.

[32] A. G. Leal-Junior et al., "Optimizing linearity and sensitivity of 3D-printed diaphragms with chirped FBGs in CYTOP fibers," *IEEE Access*, vol. 8, pp. 31983–31991, 2020, doi: 10.1109/ACCESS.2020.2973187.

[33] V. Q. Nguyen, C.-C. Chiang, and L. Tsai, "Enhanced sensitivity of bare FBG pressure sensor based on oval-shaped 3D printed structure," *Opt. Fiber Technol.*, vol. 73, Oct. 2022, Art. no. 103022, doi: 10.1016/j.yofte.2022.103022.

[34] Z. A. Abro et al., "Development of FBG pressure sensors using FDM technique for monitoring sleeping postures," *Sens. Actuators A, Phys.*, vol. 331, Nov. 2021, Art. no. 112921, doi: 10.1016/j.sna.2021.112921.

[35] C. Hong, Y. Zhang, and L. Borana, "Design, fabrication and testing of a 3D printed FBG pressure sensor," *IEEE Access*, vol. 7, pp. 38577–38583, 2019, doi: 10.1109/ACCESS.2019.2905349.

[36] A. G. Leal-Junior, C. Marques, M. R. N. Ribeiro, M. J. Pontes, and A. Frizera, "FBG-embedded 3-D printed ABS sensing pads: The impact of infill density on sensitivity and dynamic range in force sensors," *IEEE Sensors J.*, vol. 18, no. 20, pp. 8381–8388, Oct. 2018, doi: 10.1109/JSEN.2018.2866689.

[37] G. Luppino et al., "Characterization of the response of fiber Bragg grating sensors embedded in 3D printed continuous fiberglass reinforced composite for biomedical applications," in *Proc. Int. Conf. Comput. Helping People Special Needs*, 2022, pp. 494–501.

[38] M. Kostovic et al., "A multidisciplinary approach for the designing and realization of customized high performance prostheses by continuous fiber additive manufacturing," in *Proc. Int. Conf. Comput. Helping People Special Needs*, 2022, pp. 379–386.

[39] H. Cheng-Yu, Z. A. Abro, Z. Yi-Fan, and R. A. Lakho, "An FBG-based smart wearable ring fabricated using FDM for monitoring body joint motion," *J. Ind. Textiles*, vol. 50, no. 10, pp. 1660–1673, Jun. 2021, doi: 10.1177/1528083719870204.

[40] C. Hong, C. Bao, J. Fei, Y. Zhang, and X. Wang, "Application of FBG technology in additive manufacturing: Monitoring real-time internal temperature of products," *IEEE Sensors J.*, vol. 21, no. 5, pp. 6003–6011, Mar. 2021, doi: 10.1109/JSEN.2020.3041091.

[41] S. Wang and K. Lasn, "Integration of optical fibre sensors by material extrusion 3-D printing—The effect of bottom interlayer thickness," *Mater. Des.*, vol. 221, Sep. 2022, Art. no. 110914, doi: 10.1016/j.matdes.2022.110914.

[42] S. Wang, E. Sæter, and K. Lasn, "Comparison of DOFS attachment methods for time-dependent strain sensing," *Sensors*, vol. 21, no. 20, p. 6879, Oct. 2021, doi: 10.3390/s21206879.

[43] A. Vieira, R. de Oliveira, O. Frazão, J. M. Baptista, and A. T. Marques, "Effect of the recoating and the length on fiber Bragg grating sensors embedded in polymer composites," *Mater. Des.*, vol. 30, no. 5, pp. 1818–1821, May 2009, doi: 10.1016/J.MATDES.2008.08.005.

[44] K.-T. Lau, L. Yuan, L.-M. Zhou, J. Wu, and C.-H. Woo, "Strain monitoring in FRP laminates and concrete beams using FBG sensors," *Compos. Struct.*, vol. 51, no. 1, pp. 9–20, Jan. 2001.

[45] K. T. Wan, C. K. Y. Leung, and N. G. Olson, "Investigation of the strain transfer for surface-attached optical fiber strain sensors," *Smart Mater. Struct.*, vol. 17, no. 3, Jun. 2008, Art. no. 035037, doi: 10.1088/0964-1726/17/3/035037.

[46] M. Weisbrich and K. Holschemacher, "Comparison between different fiber coatings and adhesives on steel surfaces for distributed optical strain measurements based on Rayleigh backscattering," *J. Sensors Sensor Syst.*, vol. 7, no. 2, pp. 601–608, Nov. 2018, doi: 10.5194/jsss-7-601-2018.

Davide Paloschi (Graduate Student Member, IEEE) received the B.S. and M.S. degrees in automation and control engineering from the Politecnico di Milano, Milan, Italy, in 2016 and 2018, respectively, where he is currently pursuing the Ph.D. degree with the Department of Mechanical Engineering.

From 2019 to 2020, he was a Research Fellow at the Department of Mechanical Engineering, Politecnico di Milano. His research interests include the monitoring of physiological parameters, model prediction, data analysis, and noise filtering.

Andrea Polimadei is currently a Technician with the Photonics Micro- and Nanostructures Laboratory, Research Centre of Frascati, ENEA, Frascati, RM, Italy. His research interests include distributed fiber-optic-based sensors for structural monitoring and interferometric techniques' development and applications of fiber-optic sensors in the medical field.

Sanzhar Korganbayev (Graduate Student Member, IEEE) received the B.S. and M.S. degrees in electrical and electronics engineering from Nazarbayev University, Astana, Kazakhstan, in 2016 and 2018, respectively, and the Ph.D. degree in mechanical engineering from the Politecnico di Milano, Milan, Italy, in 2022.

He is currently involved in the LEILA Project (European Research Council Grant) for the development of software for real-time temperature monitoring and intraoperative adjustment of the laser settings during tumor treatment. His research interests include fiber optic sensors and their applications for thermal and mechanical measurements.

Valerio Orsetti is currently a Mechanical Designer with DTT S.c.a.r.l. as Responsible Officer ASI (Assembly System Integration). From 2011 to 2019, he was with the FSN-TECFIS-MNF Department at ENEA Research Center of Frascati, Frascati, RM, Italy. He participated in several projects, such as the design of the sputtering plant "ENEA-2," the design of receiver tubes in the TUBOSOL project, the experimental activities of the TECVIM project, the realization of an XPS apparatus for the EUROfusion project, the risk management assessment for the RAFAEL project, and many more.

Cristina Mazzotta received the bachelor's degree in physics from the University of Bologna, Bologna, Italy, in 1995, and the Ph.D. degree in energetics from the University of Rome "La Sapienza," Rome, Italy, in 2011.

She was a Scientific Coordinator and a Leader of the FTU (Frascati Tokamak Upgrade) Diagnostic Coordinator Group and involved in EU collaborations (e.g., Joint European Torus, U.K.). She taught applied physics at the University of Brescia, Brescia, Italy. She is currently a Researcher with the Fusion and Technologies for Department of Nuclear Safety and Security, ENEA Research Center of Frascati, Rome. Her scientific production includes 180 publications or proceedings. Her main research interests include applications of Bragg fiber gratings as photosensitivity devices and plasma physics in magnetic confinement fusion with tokamak reactor and related diagnostics.

Alfredo Cigada (Member, IEEE) received the Ph.D. degree in applied mechanics from the Politecnico di Milano, Milan, Italy, in 1994.

He is currently a Professor of mechanical and thermal measurements with the Politecnico di Milano. He is also a PI of several national and international projects aimed at the development of new sensing systems, data networks, and analysis. His main research interests include the development of new measurement systems for structural health monitoring of civil structures and cultural heritage.

Michele Arturo Caponero received the bachelor's degree in physics from the University of Bari, Bari, Italy, in 1986.

He is currently a Researcher with the Photonics Micro- and Nanostructures Laboratory, Research Centre of Frascati, ENEA, Frascati, RM, Italy. His research interests include distributed fiber-optic-based sensors for structural monitoring and interferometric techniques' development.

Paola Saccomandi (Senior Member, IEEE) received the Ph.D. degree in biomedical engineering from the Università Campus Bio-Medico di Roma, Rome, Italy, in 2014.

From 2016 to 2018, she was a Post-Doctoral Researcher with the IHU Strasbourg—Institute of Image-Guided Surgery of Strasbourg, Strasbourg, France. Since 2018, she has been an Associate Professor with the Department of Mechanical Engineering, Politecnico di Milano, Milan, Italy. She is a Principal Investigator of two European Research Council Grants and several national projects. Her main research interests include fiber optic sensors and measurement systems for thermal, mechanical and biomedical measurements, biomedical imaging, and the development of light-based approaches for hyperthermal tumor treatment and monitoring.

Open Access funding provided by 'Politecnico di Milano' within the CRUI CARE Agreement